HCV infection induces ubiquitin-dependent degradation of LATS1, inactivating the Hippo pathway and upregulating transcription of the CYR61 and CTGF genes

Maria Alethea Septianastiti [1, 2], Chieko Matsui [1], Zihan Xu [1], Fransisca Puspitasari [1], Lin Deng [1], Takayuki Abe [3], Ikuo Shoji [1, #]

[1] Division of Infectious Disease Control, Center for Infectious Diseases, Kobe University Graduate School of Medicine, Kobe, Japan

[2] Faculty of Medicine, Public Health and Nursing, Universitas Gadjah Mada, Yogyakarta, Indonesia

[3] Division of Virology, Niigata University Graduate School of Medical and Dental Sciences, Niigata, Japan

Running Title: HCV inactivates Hippo via LATS1 degradation

Correspondence: Prof. Ikuo Shoji

E-mail: ishoji@med.kobe-u.ac.jp

Address: Division of Infectious Disease Control, Center for Infectious Diseases, Kobe University Graduate School of Medicine, 7-5-1 Kusunoki-cho, Chuo-ku, Kobe, Japan.

Tel.: +81-78-382-5500; Fax: +81-78-382-5519.

Word count

Abstract: 226 words

Importance: 117 words

Text: 3377

Figure: 7

Keywords: HCV, LATS1, Itch, ubiquitin, Hippo pathway, YAP1

ABSTRACT

Hepatitis C virus (HCV) is a major cause of hepatocellular carcinoma (HCC). However, the mechanisms underlying HCV-related hepatocarcinogenesis are not fully understood. The Hippo signaling pathway plays a crucial role in tumor suppression. Here, we investigated the role of the Hippo pathway in HCV-related pathogenesis. We demonstrated that HCV infection induces degradation of LATS1, a key regulator of the Hippo pathway. LATS1 degradation was reversed by a proteasomal inhibitor, but not by lysosomal inhibitors, indicating that HCV promotes proteasomal degradation of LATS1. Cell-based ubiquitylation assays revealed that HCV infection induces K6- and K11-linked polyubiquitylation of LATS1. HCV-induced degradation of LATS1 was suppressed in si-Itch-transfected Huh-7.5 cells. Moreover, Itch overexpression enhanced LATS1 polyubiquitylation in HCV-infected Huh-7.5 cells. These results suggest that the Itch ubiquitin ligase is involved in LATS1 degradation. The JNK inhibitor SP600125 abolished LATS1 polyubiquitylation, suggesting that the HCV-induced ROS/JNK/Itch pathway promotes ubiquitin-dependent proteasomal degradation of LATS1. Moreover, cell fractionation assays and immunofluorescence staining revealed that HCV infection promotes nuclear translocation of YAP1 protein, suggesting suppression of the Hippo pathway. Additionally, expression of the YAP1 target genes CYR61 and CTGF, which are involved in tissue remodeling and proliferation, was upregulated in HCV-infected Huh-7.5 cells. Taken together, these findings suggest that the HCV-induced ROS/JNK/Itch pathway promotes the ubiquitin-dependent proteasomal degradation of LATS1 protein, leading to Hippo pathway suppression and increased expression of CYR61 and CTGF.

53 **IMPORTANCE**

54 HCV infection induces ubiquitin-dependent degradation of LATS1, leading to inactivation of
55 the Hippo pathway and upregulation of the YAP1 target genes CYR61 and CTGF. We
56 provide evidence that HCV infection promotes the Itch-mediated, ubiquitin-dependent
57 degradation of LATS1, a key regulator of the Hippo pathway. HCV infection induces K6- and
58 K11-linked polyubiquitylation of LATS1, leading its degradation. HCV-induced degradation
59 of LATS1 promotes Hippo pathway inactivation and nuclear translocation of YAP1, thereby
60 upregulating expression of the CYR61 and CTGF genes. We propose a novel molecular
61 mechanism by which HCV infection induces activation of Itch and promotes LATS1
62 degradation, resulting in Hippo pathway inactivation. Understanding HCV-induced Hippo
63 pathway inactivation may lead to new strategies for preventing or treating HCV-related
64 disease.

65

66

67 **INTRODUCTION**

68 Hepatitis C virus (HCV) infection remains a global health burden, affecting an estimated 50
69 million people worldwide as of 2022 (1). HCV infection causes acute and chronic liver
70 diseases, ranging from mild illness to severe complications, including liver cirrhosis and
71 hepatocellular carcinoma (HCC). Although highly effective direct-acting antivirals (DAAs)
72 are available for HCV treatment, the risk of HCC persists even after successful viral
73 clearance (2). Notably, HCC can occur following a sustained virological response, at an
74 annual incidence of approximately 1%, surpassing that of other organ cancers (3).

75 HCV is a positive-sense, single-stranded RNA virus classified in the *Flaviviridae*
76 family, *Hepacivirus* genus. The 9.6-kb HCV RNA genome encodes a single polyprotein of
77 approximately 3,010 amino acids, which is cleaved by viral proteases and host signalases into
78 structural proteins (Core, E1, and E2) and nonstructural proteins (p7, NS2, NS3, NS4A,
79 NS5A, and NS5B) (4). As HCV infection is a major cause of HCC, understanding HCV-
80 induced modulation of cellular signaling pathways is crucial for elucidating the mechanism
81 underlying HCV-induced hepatocarcinogenesis.

82 The Hippo pathway, a key regulator of cell proliferation, apoptosis, and organ size
83 control, plays an essential role in tumor suppression. Dysregulation of the Hippo pathway is
84 implicated in the development of several cancers, including liver cancer (5–7). The Hippo
85 pathway involves a series of proteins that form a kinase cascade, including MST1/2,
86 LATS1/2, the adaptor protein SAV1, MOB1A/B, and the transcription coactivators YAP1 and
87 TEAD transcription factors. Activation of the Hippo pathway involves the phosphorylation of
88 the Serine/Threonine kinase LATS1, which in turn phosphorylates YAP1 at Ser127 and
89 promotes the binding of phosphorylated YAP1 to 14-3-3 proteins (8, 9). The association of
90 14-3-3 proteins with phosphorylated YAP1 prevents it from entering the nucleus. Conversely,

91 when the Hippo pathway is inactivated, unphosphorylated YAP1 translocates to the nucleus
92 and induces the transcription of genes responsible for cell growth (10,11).
93 Several viruses have been shown to modulate the Hippo pathway (12–15). HCV E2
94 activates the Hippo pathway by interacting with CD81, while HCV NS4B suppresses the
95 Hippo pathway via Scribble, promoting PI3K/AKT signaling and epithelial-mesenchymal
96 transition (EMT) (16,17). Similarly, Kaposi sarcoma-associated herpesvirus (KSHV) vGPCR
97 inhibits LATS1/2, enabling YAP1 nuclear translocation. Human papillomavirus 16 E6 alters
98 YAP1 localization through interaction with PDZ domains (13,15).
99 We previously reported that HCV infection activates the ROS/JNK signaling pathway
100 which in turn activates Itch, a HECT-type E3 ubiquitin ligase. Activated Itch promotes
101 polyubiquitylation of VPS4A, resulting in efficient HCV particle release (18). Notably, Itch
102 has been shown to promote the proteasomal degradation of LATS1, a critical component of
103 the Hippo pathway (19,20).
104 In this study, we investigate the Hippo pathway's role in HCV-related pathogenesis.
105 We demonstrate that HCV infection promotes the ubiquitin-dependent degradation of LATS1.
106 We also demonstrate that Itch plays an important role in HCV-induced polyubiquitylation of
107 LATS1, leading to Hippo pathway suppression and thereby contributing to HCV
108 pathogenesis.
109
110 **RESULTS**
111 **HCV promotes proteasomal degradation of LATS1 protein**
112 To investigate the Hippo signaling pathway's role in HCV-related pathogenesis, we examined
113 LATS1 protein levels in HCV J6/JFH1-infected Huh-7.5 cells. Immunoblot analysis revealed
114 a reduction in LATS1 protein levels in HCV-infected cells at both 2and 4 days post-infection
115 (Fig. 1A, first panel, lanes 2 and 4). However, reverse-transcription quantitative polymerase

116 chain reaction (RT-qPCR) analysis showed increased LATS1 mRNA levels (Fig. 1B),
117 indicating that HCV-induced reduction of LATS1 protein levels is not due to suppression of
118 LATS1 mRNA expression.

119 To further elucidate the mechanism underlying the HCV-induced reduction of LATS1,
120 we treated HCV-infected Huh-7.5 cells with two lysosomal inhibitors: NH_4Cl and
121 Bafilomycin A1. However, neither inhibitor restored LATS1 protein levels in HCV-infected
122 cells (Fig. 1C, first panel, lane 6; Fig. 1D, first panel, lane 6). Moreover, small interfering
123 RNA (siRNA)-mediated knockdown of LAMP2A, a key protein involved in chaperone-
124 mediated autophagy, also failed to restore LATS1 protein levels in HCV-infected cells (Fig.
125 1E, first panel, lane 4). These results suggest that HCV induces LATS1 reduction through a
126 pathway independent of lysosomal degradation.

127 To determine whether HCV infection promotes proteasomal degradation of LATS1,
128 we treated the cells with the proteasome inhibitor clasto-lactacystin β-lactone. Immunoblot
129 analysis revealed that clasto-lactacystin β-lactone restored LATS1 protein levels in HCV-
130 infected cells (Fig. 1F, first panel, lane 6). These results suggest that HCV infection promotes
131 proteasomal degradation of LATS1.

132

133 **HCV induces K6- and K11-linked polyubiquitylation of LATS1**

134 To investigate whether HCV infection promotes polyubiquitylation of LATS1, we
135 performed a cell-based ubiquitylation assay. Huh-7.5 cells were infected with HCV J6/JFH1
136 and subsequently transfected with pCAG-FLAG−LATS1 along with either pRK5-HA−
137 ubiquitin (Ub) wild-type or pRK5-HA−Ub mutants containing only a single lysine residue at
138 K6, K11, K27, K29, K33, K48, or K63. The cell-based ubiquitylation assays showed that
139 LATS1 was polyubiquitylated wild-type Ub, K6−Ub, and K11−Ub (Fig. 2, first panel, lanes

140 11, 12, and 13). These findings suggest that HCV infection promotes K6- and K11-linked
141 polyubiquitylation of LATS1.
142
143 **E3 ligase Itch, but not WWP1, plays a crucial role in HCV-induced polyubiquitylation**
144 **and degradation of LATS1**
145 To determine whether HCV-induced LATS1 polyubiquitylation depends specifically on Itch
146 ubiquitin ligase, we generated an inactive mutant Itch by mutating cysteine 868 to alanine
147 (pCAG-FLAG-Itch C868A), which abolishes E3 ligase activity. Huh-7.5 cells were co-
148 transfected with pCAG-Myc-LATS1, pRK5-HA−Ub, and either pCAG-FLAG-Itch or pCAG-
149 FLAG-Itch C868A. Immunoblot analysis revealed that LATS1 polyubiquitylation was
150 increased upon co-transfection with pCAG-FLAG-Itch (Fig. 3A, first panel, lane 2) but not
151 with the inactive mutant (Fig. 3A, first panel, lane 3). These results suggest that Itch mediates
152 the polyubiquitylation of LATS1.
153 To determine whether other E3 ubiquitin ligases in the HECT family, such as WWP1,
154 also play a role in the polyubiquitylation of LATS1, we performed a cell-based ubiquitylation
155 assay using wild-type pCAG-FLAG−WWP1 and the inactive mutant pCAG-FLAG−WWP1
156 C890A. Immunoblot analysis showed that LATS1 ubiquitylation was increased upon co-
157 transfection with wild-type pCAG-FLAG-WWP1 (Fig. 3B, first panel, lane 2), while the
158 inactive mutant abolishes this effect (Fig. 3B, first panel, lane 3). Next, we examined whether
159 HCV-induced LATS1 ubiquitylation is mediated by Itch or WWP1 in HCV-infected cells.
160 Mock- and HCV-infected Huh-7.5 cells were co-transfected with pRK5-HA−Ub, pCAG-
161 Myc-LATS1, and either pCAG-FLAG-Itch or pCAG-FLAG−WWP1. The cell-based
162 ubiquitylation assay revealed that HCV infection enhanced LATS1 polyubiquitylation when
163 Itch was overexpressed compared to when WWP1 was overexpressed (Fig. 3C, first panel,
164 lanes 5 and 6).

165 To verify Itch's role in HCV-induced LATS1 polyubiquitylation and degradation, we
166 performed siRNA-mediated knockdown of either Itch or WWP1 in HCV-infected cells.
167 Immunoblot analysis demonstrated that knockdown of Itch restored LATS1 protein levels
168 (Fig. 3D, first panel, lanes 2 and 4), whereas knockdown of WWP1 further decreased LATS1
169 protein levels (Fig. 3E, first panel, lanes 2 and 4). These findings suggest that Itch is
170 responsible for HCV-induced ubiquitin-dependent degradation of LATS1.

171

172 **HCV-induced ROS/JNK/Itch signaling pathway plays a role in polyubiquitylation of**
173 **LATS1**

174 To further determine whether the HCV-induced ROS/JNK/Itch signaling pathway is
175 involved in the polyubiquitylation of LATS1, we treated cells with the JNK inhibitor
176 SP600125 and assayed for LATS1 polyubiquitylation. Immunoblot analysis revealed that the
177 JNK inhibitor SP600125 disrupted HCV-induced Itch-mediated LATS1 polyubiquitylation
178 (Fig. 4, first panel, lane 6). These results suggest that the HCV-induced ROS/JNK/Itch
179 pathway promotes polyubiquitylation of LATS1.

180

181 **HCV infection promotes translocation of YAP1 from the cytoplasm to the nucleus.**

182 LATS1 is the protein kinase that phosphorylates YAP1 at Ser127 and activates the Hippo
183 signaling pathway. Therefore, we hypothesized that HCV-induced degradation of LATS1
184 may suppress the Hippo pathway. To assess this hypothesis, we performed immunoblot
185 analysis of components of the Hippo pathway, LATS1 and YAP1, in mock- and HCV-
186 infected Huh-7.5 cells. Immunoblot analysis revealed that HCV infection promoted LATS1
187 degradation (Fig. 5A, first panel, lane 2), accompanied by a reduction in phosphorylated
188 LATS1 at Ser 909 (Fig. 5A, second panel, lane 2), suggesting that active LATS1 is decreased
189 in HCV-infected cells. The decrease in pLATS1 at Ser 909 subsequently resulted in reduced

190 YAP1 phosphorylation at Ser 127 (Fig. 5A, third panel, lane 2), whereas total YAP1 levels
191 remained unchanged (Fig. 5A, fourth panel, lane 2). These results suggest that HCV infection
192 reduced LATS1 and phosphorylated LATS1 at S909, resulting in decreased YAP1
193 phosphorylation at Ser 127, thereby inactivating the Hippo pathway.

194 To determine whether unphosphorylated YAP1 translocates to the nucleus, we
195 performed a cell fractionation assay coupled with immunoblot analysis. The assay revealed
196 an increased nuclear fraction of YAP1 in HCV-infected cells (Fig. 5B, first panel, lane 4)
197 compared to mock-infected cells (Fig. 5B, first panel, lane 3). Furthermore,
198 immunofluorescence staining revealed that YAP1 was predominantly localized to the nucleus
199 in HCV-infected Huh-7.5 cells (Fig. 5C, second panel), whereas YAP1 was more
200 cytoplasmically distributed in mock-infected cells (Fig. 5C, first panel). These results suggest
201 that HCV infection promotes LATS1 degradation, leading to reduced YAP1 phosphorylation
202 and facilitating YAP1 nuclear translocation, thereby inactivating the Hippo pathway.

203

204 **mRNA levels of YAP1 target genes are upregulated upon HCV infection**

205 To determine whether HCV-induced nuclear translocation of YAP1 affects downstream gene
206 expression, we performed RT-qPCR to measure the mRNA levels of canonical YAP1 target
207 genes, CYR61 and CTGF, in HCV-infected cells. RT-qPCR showed that HCV infection
208 significantly increased the mRNA levels of CYR61 and CTGF (Fig. 6A and 6B).

209 To determine whether HCV-induced upregulation of CYR61 and CTGF depends
210 specifically on YAP1 nuclear translocation, we used siRNA to knock down YAP1 expression
211 in HCV-infected Huh-7.5 cells. YAP1 mRNA levels were successfully reduced by
212 approximately 80% (Fig. 6C). Under HCV-infected conditions, the relative mRNA levels of
213 CYR61 and CTGF were significantly lower in siYAP1-transfected cells (Fig. 6D and 6E).
214 These results suggest that HCV promotes the upregulation of CYR61 and CTGF via YAP1

215 nuclear translocation. CYR61 and CTGF are known to play roles in tissue remodeling and
216 cell proliferation, suggesting that the HCV-induced upregulation of CYR61 and CTGF genes
217 may contribute to HCV-related pathogenesis.

218 In summary, we propose the model shown in Fig. 7. Under normal conditions, the
219 Hippo pathway remains active when LATS1 phosphorylates YAP1, and phosphorylated
220 YAP1 is retained in the cytoplasm. In HCV infection, HCV activates the ROS/JNK/Itch
221 pathway. Active Itch induces the polyubiquitylation and proteasomal degradation of LATS1.
222 The degradation of LATS1 inhibits YAP1 phosphorylation and promotes YAP1 nuclear
223 translocation, thereby upregulating transcription of the YAP1 target genes, CYR61 and
224 CTGF. HCV-induced suppression of the Hippo pathway may play a role in HCV
225 pathogenesis.

226

227 **DISCUSSION**

228 In this study, we found that HCV infection induced the degradation of LATS1 protein, a
229 serine/threonine kinase essential for regulating the tumor-suppressive Hippo pathway (Fig.
230 1). We demonstrated that HCV infection promoted polyubiquitylation and proteasomal
231 degradation of LATS1 (Fig. 2). In particular, our results showed that HCV infection induced
232 K6- and K11-linked polyubiquitylation of LATS1. We also demonstrated that HCV infection
233 promoted degradation of LATS1, which inactivated the Hippo pathway and facilitated YAP1
234 nuclear translocation (Fig. 5), and that HCV infection induced the upregulation of canonical
235 YAP1 target genes, CYR61 and CTGF (Fig. 6).

236 Both CYR61 and CTGF are crucial for hepatocellular carcinoma (HCC) progression,
237 exhibiting higher expression in HCC tissues than in normal liver tissues (21). CYR61 and
238 CTGF act as adhesive substrates that stimulate fibroblast signaling, enhancing angiogenesis
239 and wound healing (22). Notably, elevated CTGF levels in human HCCs have also been

240 linked to poor clinical outcomes (23). We obtained evidence suggesting that HCV infection
241 inactivates the Hippo pathway, leading to the upregulation of CYR61 and CTGF expression,
242 thereby contributing to HCC progression.

243 Our findings further elucidate the upstream regulatory mechanisms underlying HCV-
244 induced inactivation of the Hippo pathway. We demonstrated that HCV infection promotes
245 K6- and K11-linked polyubiquitylation and proteasomal degradation of LATS1. Previous
246 studies suggest that all non-K63 linkages, including K6, K11, K27, K29, and K33, can target
247 protein for proteasomal degradation (24, 25).

248 The NEDD4 subfamily of HECT-type E3 ubiquitin ligases is characterized by
249 multiple WW domains that specifically interact with the PPxY domain of LATS1. Notably,
250 certain members of this subfamily have been identified as key regulators of LATS1 protein
251 stability (19, 20, 24, 25). We hypothesized that the NEDD4 subfamily, such as Itch or
252 WWP1, is involved in HCV-induced polyubiquitylation and proteasomal degradation of
253 LATS1. Our results suggest that Itch, but not WWP1, plays a crucial role in HCV-induced
254 degradation of LATS1 protein (Figs. 3 and 4). Both Itch and WWP1 contributed to LATS1
255 polyubiquitylation in mock-infected cells. Importantly, siRNA-mediated knockdown of Itch
256 restored LATS1 protein in HCV-infected cells. In contrast, siRNA-mediated knockdown of
257 WWP1 further reduced LATS1 protein levels (Fig. 3E). Notably, condition-specific
258 regulatory shifts have been observed in some proteins. For example, the tumor suppressor
259 p53 is primarily degraded by Murine Double Minute 2 (Mdm2) under normal conditions,
260 whereas in HPV16 E6-positive cancer cells, degradation occurs entirely via the E6-AP
261 pathway instead of Mdm2 (26). These observations raise the possibility that HCV infection
262 predominantly facilitates Itch-mediated ubiquitylation and degradation of LATS1 via as-yet-
263 undetermined mechanisms. Further investigation is required to elucidate the details of these
264 regulatory mechanisms.

265 We previously showed that HCV activates the ROS/JNK signaling pathway, which
266 activates Itch and facilitates polyubiquitylation of VPS4A, enhancing HCV release (2). In this
267 study, we demonstrated evidence suggesting that HCV-induced ROS/JNK/Itch activation
268 promotes the ubiquitin-dependent degradation of LATS1, contributing to the inactivation of
269 the Hippo pathway and nuclear translocation of YAP1, thereby upregulating CYR61 and
270 CTGF genes. This study represents, to our knowledge, the first demonstration that HCV-
271 induced ROS/JNK/Itch activation promotes Hippo pathway inactivation, leading to
272 upregulation of CYR61 and CTGF genes. These insights contribute to our understanding of
273 the molecular mechanisms underlying HCV pathogenesis and hepatocarcinogenesis,
274 highlighting potential targets for therapeutic intervention.
275

276 **MATERIALS AND METHODS**

277 **Cell culture and viruses**

278 Human hepatoma cell line Huh-7.5 cells were generously provided by Dr. Charles M. Rice
279 (The Rockefeller University, New York, NY). The cells were cultured in Dulbecco's Modified
280 Eagle's Medium (DMEM) (high glucose) containing L-glutamine and phenol red (044-
281 29765; Fuji Film Wako Pure Chemical Industries, Osaka, Japan) supplemented with 50 IU/ml
282 penicillin, 50 μg/ml streptomycin (15-140-122; Gibco, Grand Island, NY), 10% heat-
283 inactivated fetal bovine serum (FBS) (S1760-500; Biowest, Nuaillé, France), and 0.1 mM
284 non-essential amino acids (Invitrogen, Carlsbad, CA). Cells were cultured at 37°C in a 5%
285 CO_2 incubator. Cells were washed with PBS (-) solution (05913; Nissui Pharmaceutical Co.,
286 Ltd., Tokyo, Japan) and transfected with plasmid DNA using FuGENE 6 transfection reagents
287 (E269A; Promega, Madison, WI). The pFL-J6/JFH1 plasmid, encoding the entire viral
288 genome of the chimeric HCV-2a strain J6/JFH1, was also kindly provided by Dr. Charles M.
289 Rice. HCV genome RNA was synthesized *in vitro* using pFL-J6/JFH1 as a template and

290 subsequently transfected into Huh-7.5 cells via electroporation. The virus produced in the
291 culture supernatant was then used for infection experiments (27, 28).

292

293 **Expression plasmids**

294 The cDNA fragment of LATS1 was amplified by PCR using the following specific primers:
295 forward 5'-TCGAGCTCAGCGGCCATGAAGAGGAGTGAAAAGCCAG-3' and reverse
296 5'-TCGAGCTCAGCGGCCATGAAGAGGAGTGAAAAGCCAG-3'. The amplified PCR
297 product was purified and inserted into the NotI site of the pCAG-FLAG plasmid using the In-
298 Fusion HD Cloning Kit (Clontech, Mountain View, CA). The sequences of the inserts were
299 verified by sequencing (Eurofins Genomics, Tokyo, Japan).

300 To construct the pCAG-Myc-LATS1 expression plasmid, pCAG-FLAG-LATS1 was
301 used as a template and the cDNA fragment of LATS1 was amplified using the following
302 specific primers: forward 5'-
303 AAGGTACCATGGAGCAAAAGCTCATTTCTGAAGAGGACCTGATGAAGAGGAGTG
304 AAAAGCCA-3' and reverse 5'-TTAGATCTTCAAACATATACTAGATCGCGATT-3'. The
305 amplified PCR product was purified and inserted into the KpnI and BglII sites of the pCAG-
306 MCS2 vector using the Ligation-Convenience Kit (Nippon Gene, Tokyo, Japan).

307 The expression plasmids pCAG-FLAG-Itch and pCAG-FLAG−WWP1 were
308 described previously (29). The C890A point mutant of WWP1 was generated by overlap
309 extension PCR using pCAG-FLAG−WWP1 as a template and the following specific primers:
310 forward 5'-AGAAGCCATACAGCTTTTAATCGCTTG-3' and reverse 5'-
311 CAAGCGATTAAAAGCTGTATGGCTTCT-3'. The sequences of the inserts were verified
312 by sequencing (Eurofins Genomics).

313 N-terminal HA-tagged ubiquitin (Ub) expression plasmids, including pRK5-HA−Ub-
314 WT, pRK5-HA−Ub-K6, pRK5-HA−Ub-K11, pRK5-HA−Ub-K27, pRK5-HA−Ub-K29,

315 pRK5-HA−Ub-K33, pRK5-HA−Ub-K48, and pRK5-HA−Ub-K63, were purchased from
316 Addgene (Watertown, MA).
317
318 **Antibodies and reagents**
319 The mouse monoclonal antibodies (MAbs) used in this study were anti-FLAG (M2) MAb
320 (F3165, Sigma-Aldrich), anti-β-actin (A5441; Sigma-Aldrich) anti-c-Myc (9E10) Mab (sc-
321 40; Santa Cruz Biotechnology, Dallas, TX), anti-Itch Mab (611198, BD Transduction
322 Laboratories, San Jose, CA), anti-Histone H3 (1G1) MAb (sc-517576; Santa Cruz
323 Biotechnology), and anti-YAP (63.7) MAb (sc-101199; Santa Cruz Biotechnology). The
324 rabbit monoclonal antibody used in this study was anti-LATS1 (C66B5) MAb (3477; Cell
325 Signaling Technology). The rabbit polyclonal antibodies (PAbs) used in this study included
326 anti-HA PAb (H-6908; Sigma-Aldrich), anti-phospho-LATS1 (Ser909) PAb (9157; Cell
327 Signaling Technology), anti-LAMP2A PAb (ab18528; Abcam, Cambridge, UK), anti-YAP
328 PAb (4912; Cell Signaling Technology), anti-phospho-YAP (Ser127) (4911; Cell Signaling
329 Technology), anti-NS5A PAb (2914-1; a kind gift from T. Wakita, National Institute of
330 Infectious Diseases, Tokyo, Japan), and anti-IκBα PAb (9242; Cell Signaling Technology).
331 Horseradish peroxidase (HRP)-conjugated anti-mouse IgG (7076S; Cell Signaling
332 Technology) and HRP-conjugated anti-rabbit IgG (7074S; Cell Signaling Technology) were
333 used as secondary antibodies. Clasto-lactacystin β-lactone (031-18201; Wako) was used as a
334 proteasome inhibitor. Ammonium chloride (NH_4Cl) was purchased from Fuji Film Wako
335 Pure Chemical Industries.
336
337 **Immunoblot analysis**
338 Immunoblot analysis was conducted as previously described (30). Cell lysates were separated
339 using 8% or 15% sodium dodecyl sulfate−polyacrylamide gel electrophoresis (SDS-PAGE)

340 and transferred onto a 0.45 μm Immobilon-P polyvinylidene difluoride (PVDF) membrane
341 (Millipore, Billerica, MA). The membranes were incubated with a primary antibody, followed
342 by an HRP-conjugated secondary antibody. Positive bands were detected using Amersham
343 enhanced chemiluminescence (ECL) western blotting detection reagents (Cytiva, RPN2106;
344 Sigma-Aldrich). Band intensities were quantified using ImageJ software (version 1.54h).
345

346 **Cell-based ubiquitylation assay and immunoprecipitation**

347 Cell-based ubiquitylation assays and immunoprecipitation experiments were performed as
348 previously described (29). Cultured cells were lysed in a lysis buffer containing 50 mM
349 HEPES (pH 7.5), 150 mM NaCl, 1 mM EDTA, 1% NP-40, 1 mM DTT, 1 mM PMSF, 10 mM
350 pyrophosphate, 10 mM glycerophosphate, 50 mM NaF, 1.5 mM Na_3VO_4, and a complete™,
351 EDTA-free protease inhibitor cocktail (Roche Molecular Biochemicals, Mannheim,
352 Germany). After sonication, the lysates were immunoprecipitated using either anti-FLAG M2
353 affinity gel (A2220; Sigma-Aldrich) or Protein A-Sepharose 4 Fast Flow (GE17-5280-04; GE
354 Healthcare, Buckinghamshire, UK) pre-incubated with the appropriate antibodies.
355 Immunoprecipitation was carried out at 4°C for 4 h or overnight. The immunoprecipitates
356 were washed five times with the lysis buffer and analyzed by immunoblotting using specific
357 antibodies, including anti-HA for ubiquitylation assays.
358

359 **Cell fractionation assay**

360 Cytoplasmic and nuclear extracts from HCV-infected and mock-infected Huh-7.5 cells were
361 separated using NE-PER™ Nuclear and Cytoplasmic Extraction Reagents (78835; Thermo
362 Fisher Scientific) following the manufacturer's instructions. The resulting lysates were then
363 analyzed by immunoblotting.
364

365 **RNA extraction and RT-qPCR**

366 Total RNA was extracted using the ReliaPrep RNA Cell Miniprep System (Promega)
367 following the manufacturer's protocol. The GoScript Reverse Transcription System
368 (Promega) was used for cDNA synthesis. RT-qPCR was performed on a StepOnePlus Real-
369 Time PCR System (Applied Biosystems, Foster City, CA) using TB Green Premix Ex Taq II
370 (TaKaRa Bio, Shiga, Japan) with SYBR Green chemistry. The primer sequences used were as
371 follows: LATS1 (forward: 5'-CTCTGCACTGGCTTCAGATG-3', reverse: 5'-
372 TCCGCTCTAATGGCTTCAGT-3'); YAP1 (sense: 5'- CCCGACAGGCCAGTACTGAT-3',
373 antisense: 5'-CAGAGAAGCTGGAGAGGAATGAG-3'CYR61 (sense: 5'-
374 GGTCAAAGTTACCGGGCAGT-3', antisense: 5'-GGAGGCATCGAATCCCAGC-3'); and
375 CTGF (forward: 5'-CCTGGTCCAGACCACAGAGT-3', reverse: 5'-
376 ATGTCTTCATGCTGGTGCAG-3'). Expression of the human GAPDH gene was measured
377 as an internal control using the primers 5'-GCCATCAATGACCCCTTCATT-3' (forward)
378 and 5'-TCTCGCTCCTGGAAGATGG-3'(reverse).

379

380 **RNA interference and stable knockdown cells**

381 The generation of shControl and shLAMP2A cells was described previously (31). HCV-
382 infected and uninfected Huh-7.5 cells were transfected with either Itch siRNA (SI00141085;
383 Qiagen,). WWP1 siRNA (JP00049582-001; Sigma-Aldrich), YAP siRNA (WD11034049-
384 001; Sigma-Aldrich), or negative-control scrambled siRNA (1027281; Qiagen) using
385 Lipofectamine RNAiMAX transfection reagent (Life Technologies, Carlsbad, CA) according
386 to the manufacturer's instructions. The siRNA sequences were as follows: siWWP1, 5'-
387 CUUCUACGAUCAUCAACUCTT-3'; siYAP1, 5'-TTCTTTATCTAGCTTGGTGGC-3'. All
388 siRNAs were transfected once.

389

390 **Immunofluorescence staining**

391 Huh-7.5 cells cultured on glass coverslips were fixed with 4% paraformaldehyde at room
392 temperature (RT) for 15 min. After being washed with phosphate-buffered saline (PBS)
393 (05913; Nissui Pharmaceutical Co., Ltd.), the cells were permeabilized with PBS containing
394 0.1% Triton X-100 for 15 min at RT. To block nonspecific binding, the cells were incubated
395 in PBS containing 1% bovine serum albumin (BSA) (01859-47; Nacalai Tesque) for 60 min.
396 The cells were then incubated with 1% BSA in PBS containing mouse anti-YAP monoclonal
397 antibody and rabbit anti-NS5A polyclonal antibody at RT for 60 min. Afterward, the cells
398 were washed three times with PBS and further incubated with 1% BSA in PBS containing
399 Alexa Fluor™ 594-conjugated anti-mouse IgG (A11005; Invitrogen) and Alexa Fluor™ 488-
400 conjugated anti-rabbit IgG (A11008; Invitrogen) at RT for 60 min. Finally, the cells were
401 washed four times with PBS, mounted on glass slides, and examined using a confocal
402 microscope (LSM 700, Carl Zeiss, Oberkochen, Germany).

403

404 **Statistical analysis**

405 Results were expressed as means ± standard error of the mean (SEM). Statistical significance
406 was evaluated using Student's t-test and was defined as a P value of <0.05.

407

408 **Data Availability Statement**

409 All data are presented in the main figures. The data that support the findings of this study is
410 available at bioRxiv (https://www.biorxiv.org/). Raw sequencing data, microscopy images,
411 materials, and sequence information are available upon request. Correspondence and requests
412 for materials should be addressed to Professor Ikuo Shoji.

413

414 **ACKNOWLEDGEMENTS**

We sincerely appreciate Dr. C. M Rice (The Rockefeller University, New York) for generously providing the Huh-7.5 cells and pFL-J6/JFH1 plasmid. We also thank Y. Kozaki for her valuable secretarial assistance.

FUNDING INFORMATION

This research was supported by grants for Basic and Clinical Research on Hepatitis from the Japan Agency for Medical Research and Development (AMED) grant No. 23fk0210090s1203 and 20fk0210040s0703, a KAKENHI grant No. 20K07514 and 22K15470, and the Program for the Nurturing of Next Generation Leaders Guiding Medical Innovation in Asia, funded by the Ministry of Education, Culture, Sports, Science, and Technology (MEXT) of Japan.

AUTHOR CONTRIBUTIONS

C.M. and I.S. conceived and designed the experiments. S.MA and C.M. carried out most of the experiments. ZX., F.P., C.M., L.D., and T.A. assisted the constructions and the data analysis. S.MA., C.M, and I.S. wrote the manuscript.

DECLARATION OF INTERESTS

The authors declare no conflict of interest.

435 **FIGURE LEGENDS**

436 **Figure 1. HCV induces proteasomal degradation of LATS1.**

437 (A) Huh-7.5 cells were infected with HCV J6/JFH1 at a multiplicity of infection (MOI) of 2.
438 Cells were cultured and harvested at 2 and 4 days post-infection (dpi). Immunoblot analysis
439 was performed using the indicated antibodies, with β-actin levels serving as a loading control.
440 (B) Huh-7.5 cells were infected with HCV J6/JFH1 at an MOI of 2, cultured, and harvested at
441 2 and 4 dpi. Total cellular RNA was extracted, and LATS1 mRNA levels were quantified
442 using RT-qPCR. GAPDH mRNA levels were used for normalization. The value for day 2 in
443 the mock-infected group was expressed as 1.0. Data are presented as means ± SEM from
444 three independent experiments; p-value < 0.05 (*) was significant, compared with the
445 controls. (C) Huh-7.5 cells were infected with HCV J6/JFH1 at an MOI of 2, followed by
446 treatment with NH_4CL for 12 h. Immunoblotting was performed with the specified
447 antibodies, and β-actin levels served as a loading control. (D) Huh-7.5 cells were infected
448 with HCV J6/JFH1 at an MOI of 2, followed by treatment with Bafilomycin A1 for 12 h.
449 Immunoblotting was performed with the indicated antibodies, and β-actin was used as a
450 loading control.
451 (E) shControl- and shLAMP2A-Huh-7.5 cells were infected with HCV J6/JFH1 at an MOI of
452 2. Immunoblot analysis was performed using indicated antibodies with β-actin as a loading
453 control. (F) Huh-7.5 cells were infected with HCV J6/JFH1 at an MOI of 2. Cells were
454 treated with 30 μM clasto-lactacystin β-lactone for 12 h, harvested, and analyzed by
455 immunoblotting using the indicated antibodies. β-actin was used as a loading control.
456

457 **Figure 2. HCV induces K6- and K11-linked polyubiquitylation of LATS1.**

458 Huh-7.5 cells were infected with HCV J6/JFH1 at an MOI of 0.5 and co-transfected with
459 pCAG-FLAG-LATS1 together with the indicated HA-tagged ubiquitin mutant plasmids. At 2

460 days post-transfection, cells were harvested and cell lysates were immunoprecipitated with
461 anti-FLAG beads, followed by immunoblotting with the indicated antibodies. Input samples
462 were also analyzed by immunoblotting with the indicated antibodies, and β-actin was used as
463 a loading control.
464
465 **Figure 3. E3 ligase Itch, but not WWP1, plays a crucial role in HCV-induced**
466 **polyubiquitylation and degradation of LATS1.**
467 (A) Huh-7.5 cells were co-transfected with pCAG-Myc-LATS1, pRK5-HA-Ubiquitin,
468 together with either pCAG-FLAG-Itch WT or pCAG-FLAG-Itch C868A. At 2 days post-
469 transfection, the cells were harvested. The cell lysates were immunoprecipitated with anti-c-
470 Myc antibody-conjugated Sepharose A beads, followed by immunoblotting with the indicated
471 antibodies. Input samples were also analyzed by immunoblotting. β-actin was used as a
472 loading control. (B) Huh-7.5 cells were co-transfected with pCAG-Myc-LATS1, pRK5-
473 HA−Ubiquitin, together with either pCAG-FLAG−WWP1 WT or pCAG-FLAG−WWP1
474 C890A. At 2 days post-transfection, cells were harvested. The cell lysates were
475 immunoprecipitated with anti-c-Myc antibody−conjugated Sepharose A beads, followed by
476 immunoblotting with the indicated antibodies. Input samples were also immunoblotted, with
477 β-actin serving as a loading control.
478 (C) Huh-7.5 cells were infected with HCV J6/JFH1 at an MOI of 1 and co-transfected with
479 pCAG-Myc-LATS1 and pRK5-HA−Ubiquitin, together with either pCAG-FLAG-Itch or
480 pCAG-FLAG−WWP1. Cell lysates were immunoprecipitated using anti-c-Myc
481 antibody−conjugated Sepharose A beads, followed by immunoblotting with the indicated
482 antibodies. Input samples were also analyzed. β-actin was used as a loading control. (D) Huh-
483 7.5 cells (3×10^5 cells per well in a 12-well plate) were transfected with 48 pmol of either
484 control siRNA or Itch-specific siRNA. After 24 h, the cells were infected with HCV J6/JFH1

485 at an MOI of 2 and harvested at 2 days post-infection. The samples were analyzed by
486 immunoblotting with the indicated antibodies. β-actin was used as a loading control. (E) Huh-
487 7.5 cells (3×10^5 cells per well in a 12-well plate) were transfected with 48 pmol of either
488 control siRNA or WWP1-specific siRNA. At 24 h after siRNA-transfection, the cells were
489 infected with HCV J6/JFH1 at an MOI of 2. Cells were harvested at 2 days post-infection,
490 and the samples were subjected to immunoblotting with the indicated antibodies. β-actin was
491 used as a loading control.
492
493 **Figure 4. HCV-induced ROS/JNK/Itch signaling pathway plays a role in**
494 **polyubiquitylation of LATS1 protein**
495 Huh-7.5 cells were infected with HCV J6/JFH1 at an MOI of 1, then co-transfected with
496 pCAG-Myc-LATS1 and pRK5-HA-ubiquitin, together with pCAG-FLAG-Itch. After 2 days,
497 the cells were harvested with or without pretreatment with JNK inhibitor SP6000125 (30 μM
498 for 30 h), and the lysates were immunoprecipitated with anti-c-Myc antibody−conjugated
499 Sepharose A beads, followed by immunoblotting with the indicated antibodies. Input samples
500 were also analyzed by immunoblotting. β-actin was used as a loading control.
501
502 **Figure 5. HCV infection promotes the translocation of YAP1 from the cytoplasm to the**
503 **nucleus.**
504 (A) Huh-7.5 cells were infected with HCV J6/JFH1 at an MOI of 2. Following infection, the
505 cells were harvested and analyzed by immunoblotting using antibodies against components of
506 the Hippo pathway. (B) Huh-7.5 cells were infected with HCV J6/JFH1 at an MOI of 2. At 4
507 days after infection, the cells were harvested and subjected to cell fractionation analysis. Ikβα
508 was used as a loading control for the cytoplasmic fraction, and Histone H3 was used as a
509 loading control for the nuclear fraction. (C) Huh-7.5 cells were plated and cultured for 12 h

510 and infected with HCV J6/JFH1 at an MOI of 2. Cells were stained with anti-YAP1
511 monoclonal antibody followed by Alexa Fluor 594−conjugated goat anti-mouse IgG (red) and
512 anti-NS5A polyclonal antibody followed by Alexa Fluor 488−conjugated goat anti-rabbit IgG
513 (green). Nuclei were counterstained with Hoechst 33342 (blue). Images were acquired using
514 scanning laser confocal microscopy and processed with ImageJ software.
515
516 **Figure 6. The mRNA levels of YAP1 target genes are significantly upregulated upon**
517 **HCV infection.**
518 (A, B) Huh-7.5 cells were infected with HCV J6/JFH1 at an MOI of 2. Cells were cultured
519 and harvested at 2 and 4 days post-infection (dpi). Total cellular RNA was subsequently
520 extracted, and the mRNA levels of CYR61 and CTGF were quantified by RT-qPCR. GAPDH
521 mRNA levels were used for normalization. The mRNA level for day 2 in the mock-infected
522 group was arbitrarily expressed as 1.0. Data are presented as means ± SEM from three
523 independent experiments. A p-value < 0.05 (*) was considered significant. (C−E) Huh-7.5
524 cells at (1.8×10^5 cells per well in a 24-well plate) were transfected with 24 pmol of either
525 control siRNA or YAP siRNA. At 24 h after siRNA transfection, the cells were infected with
526 HCV J6/JFH1 at an MOI of 2, cultured, and harvested at the indicated time points. Total RNA
527 was extracted, and YAP1, CYR61, and CTGF mRNA levels were quantified by RT-qPCR,
528 normalized to GAPDH mRNA levels. The mRNA level at day 2 in the mock-infected group
529 was arbitrarily set to 1.0. Data are expressed as mean ± SEM from three independent
530 experiments. A p-value < 0.05 (*) was considered significant.
531
532 **Figure 7. A proposed model of HCV-induced inactivation of the Hippo pathway and**
533 **HCV-related pathogenesis.**

Under normal conditions, the Hippo pathway remains predominantly active, with LATS1 phosphorylating YAP1, thereby retaining YAP1 in the cytoplasm and preventing its nuclear entry. HCV infection activates the ROS/JNK/Itch signalling pathway, which is crucial for HCV particle release. Activation of the ROS/JNK/Itch signalling pathway leads to the phosphorylation and enhanced activity of Itch ubiquitin ligase. Activated Itch promotes the ubiquitin-dependent proteasomal degradation of LATS1 protein, leading to the Hippo pathway inactivation. As a result, YAP1 translocates from the cytoplasm to the nucleus and upregulates the transcription of CYR61 and CTGF genes, contributing to HCV-related pathogenesis.

544 **REFERENCES**

545 1. World Health Organization. 2024. Global Hepatitis Report 2024: Action for Access in
546 Low- and Middle-Income Countries. World Health Organization, Geneva, Switzerland.

547 2. Bartenschlager R, Baumert TF, Bukh J, Houghton M, Lemon SM, Lindenbach BD,
548 Lohmann V, Moradpour D, Pietschmann T, Rice CM, Thimme R, Wakita T. 2018.
549 Critical challenges and emerging opportunities in hepatitis C virus research in an era of
550 potent antiviral therapy: Considerations for scientists and funding agencies. Virus Res
551 248:53–62.

552 3. Baumert TF, Jühling F, Ono A, Hoshida Y. 2017. Hepatitis C-related hepatocellular
553 carcinoma in the era of new generation antivirals. BMC Med 15(1):52.

554 4. Scheel TKH, Rice CM. 2013. Understanding the hepatitis C virus life cycle paves the
555 way for highly effective therapies. Nat Med 19(7):837–49.

556 5. Sohn BH, Shim JJ, Kim SB, Jang KY, Kim SM, Kim JH, Hwang JE, Jang HJ, Lee HS,
557 Kim SC, Jeong W, Kim SS, Park ES, Heo J, Kim YJ, Kim DG, Leem SH, Kaseb A,
558 Hassan MM, Cha M, Chu IS, Johnson RL, Park YY, Lee JS. 2016. Inactivation of Hippo
559 Pathway Is Significantly Associated with Poor Prognosis in Hepatocellular Carcinoma.
560 Clin Cancer Res 22(5):1256–64.

561 6. Zheng T, Wang J, Jiang H, Liu L. 2011. Hippo signaling in oval cells and
562 hepatocarcinogenesis. Cancer Lett 302(2):91–9.

563 7. Zhao B, Li L, Lei Q, Guan KL. 2010. The Hippo–YAP pathway in organ size control and
564 tumorigenesis: an updated version. Genes Dev 24(9):862–74.

565 8. Zhao B, Li L, Tumaneng K, Wang CY, Guan KL. 2010. A coordinated phosphorylation
566 by Lats and CK1 regulates YAP stability through SCF $^{\beta\text{-TRCP}}$. Genes Dev 24(1):72–85.

567 9. Zhao B, Wei X, Li W, Udan RS, Yang Q, Kim J, Xie J, Ikenoue T, Yu J, Li L, Zheng P, Ye
568 K, Chinnaiyan A, Halder G, Lai ZC, Guan KL. 2007. Inactivation of YAP oncoprotein by
569 the Hippo pathway is involved in cell contact inhibition and tissue growth control. Genes
570 Dev 21(21):2747–61.

571 10. Meng Z, Moroishi T, Guan KL. 2016. Mechanisms of Hippo pathway regulation. Genes
572 Dev 30(1):1–17.

573 11. Kwon H, Kim J, Jho E. 2022. Role of the Hippo pathway and mechanisms for controlling
574 cellular localization of YAP/TAZ. FEBS J 289(19):5798–818.

575 12. Wang Z, Lu W, Zhang Y, Zou F, Jin Z, Zhao T. 2020. The Hippo Pathway and Viral
576 Infections. Front Microbiol 10:3033.

577 13. Liu G, Yu FX, Kim YC, Meng Z, Naipauer J, Looney DJ, Liu X, Gutkind JS, Mesri EA,
578 Guan KL. 2015. Kaposi sarcoma-associated herpesvirus promotes tumorigenesis by
579 modulating the Hippo pathway. Oncogene 34(27):3536–46.

580 14. Garcia G, Paul S, Beshara S, Ramanujan VK, Ramaiah A, Nielsen-Saines K, Li MMH,
581 French SW, Morizono K, Kumar A, Arumugaswami V. 2020. Hippo Signaling Pathway
582 Has a Critical Role in Zika Virus Replication and in the Pathogenesis of
583 Neuroinflammation. Am J Pathol 190(4):844–61.

584 15. Webb Strickland S, Brimer N, Lyons C, Vande Pol SB. 2018. Human Papillomavirus E6
585 interaction with cellular PDZ domain proteins modulates YAP nuclear localization.
586 Virology 516:127–38.

587 16. Xue Y, Mars WM, Bowen W, Singhi AD, Stoops J, Michalopoulos GK. 2018. Hepatitis C
588 Virus Mimics Effects of Glypican-3 on CD81 and Promotes Development of
589 Hepatocellular Carcinomas via Activation of Hippo Pathway in Hepatocytes. Am J Pathol
590 188(6):1469–77.

591 17. Hu B, Xie S, Hu Y, Chen W, Chen X, Zheng Y, Wu X. 2017. Hepatitis C virus NS4B
592 protein induces epithelial-mesenchymal transition by upregulation of Snail. Virol J
593 14(1):83.

594 18. Deng L, Liang Y, Ariffianto A, Matsui C, Abe T, Muramatsu M, Wakita T, Maki M,
595 Shibata H, Shoji I. 2022. Hepatitis C Virus-Induced ROS/JNK Signaling Pathway
596 Activates the E3 Ubiquitin Ligase Itch to Promote the Release of HCV Particles via
597 Polyubiquitylation of VPS4A. J Virol 96(6):e01811-21. A

598 19. Salah Z, Melino G, Aqeilan RI. 2011. Negative Regulation of the Hippo Pathway by E3
599 Ubiquitin Ligase ITCH Is Sufficient to Promote Tumorigenicity. Cancer Res 71(5):2010–
600 20.

601 20. Ho KC, Zhou Z, She YM, Chun A, Cyr TD, Yang X. 2011. Itch E3 ubiquitin ligase
602 regulates large tumor suppressor 1 stability. Proc Natl Acad Sci U S A 108(12):4870–5.

603 21. Zeng ZJ. 2004. Expressions of cysteine-rich61, connective tissue growth factor and Nov
604 genes in hepatocellular carcinoma and their clinical significance. World J Gastroenterol
605 10(23):3414.

606 22. Chen CC, Chen N, Lau LF. 2001. The Angiogenic Factors Cyr61 and Connective Tissue
607 Growth Factor Induce Adhesive Signaling in Primary Human Skin Fibroblasts. J Biol
608 Chem 276(13):10443–52.

609 23. Simile MM, Latte G, Demartis MI, Brozzetti S, Calvisi DF, Porcu A, Feo CF, Seddaiu
610 MA, Daino L, Berasain C, Tomasi ML, Avila MA, Feo F, Pascale RM. 2016. Post-
611 translational deregulation of YAP1 is genetically controlled in rat liver cancer and
612 determines the fate and stem-like behavior of the human disease. Oncotarget
613 7(31):49194–216.

614 24. Yeung B, Ho KC, Yang X. 2013. WWP1 E3 Ligase Targets LATS1 for Ubiquitin-
615 Mediated Degradation in Breast Cancer Cells. PLoS ONE 8(4):e61027.

616 25. Salah Z, Cohen S, Itzhaki E, Aqeilan R. 2013. NEDD4 E3 ligase inhibits the activity of
617 the Hippo pathway by targeting LATS1 for degradation. Cell Cycle 12(24):3817–23.

618 26. Hengstermann A, Linares LK, Ciechanover A, Whitaker NJ, Scheffner M. 2001.
619 Complete switch from Mdm2 to human papillomavirus E6-mediated degradation of p53
620 in cervical cancer cells. Proc Natl Acad Sci U S A 98(3):1218-1223.

621 27. Wakita T, Pietschmann T, Kato T, Date T, Miyamoto M, Zhao Z, Murthy K, Habermann
622 A, Krausslich HG, Mizokami M, Bartenschlager R, Liang TJ. 2005. Production of
623 infectious hepatitis C virus in tissue culture from a cloned viral genome. Nat Med
624 11(7):791–6.

625 28. Bungyoku Y, Shoji I, Makine T, Adachi T, Hayashida K, Nagano-Fujii M, Ide Y, Deng L,
626 Hotta H. 2009. Efficient production of infectious hepatitis C virus with adaptive
627 mutations in cultured hepatoma cells. J Gen Virol 90(7):1681–91.

628 29. Shirakura M, Murakami K, Ichimura T, Suzuki R, Shimoji T, Fukuda K, Abe K, Sato S,
629 Fukasawa M, Yamakawa Y, Nishijima M, Moriishi K, Matsuura Y, Wakita T, Suzuki T,
630 Howley PM, Miyamura T, Shoji I. 2007. E6AP Ubiquitin Ligase Mediates Ubiquitylation
631 and Degradation of Hepatitis C Virus Core Protein. J Virol 81(3):1174–85.

632 30. Matsui C, Shoji I, Kaneda S, Sianipar IR, Deng L, Hotta H. 2012. Hepatitis C Virus
633 Infection Suppresses GLUT2 Gene Expression via Downregulation of Hepatocyte
634 Nuclear Factor 1α. J Virol 86(23):12903–11.

635 30. Yuliandari P, Matsui C, Deng L, Abe T, Mori H, Taguwa S, Ono C, Fukuhara T, Matsuura
636 Y, Shoji I. 2022. Hepatitis C virus NS5A protein promotes the lysosomal degradation of
637 diacylglycerol O-acyltransferase 1 (DGAT1) via endosomal microautophagy. Autophagy
638 Rep 1(1):264–85.

639

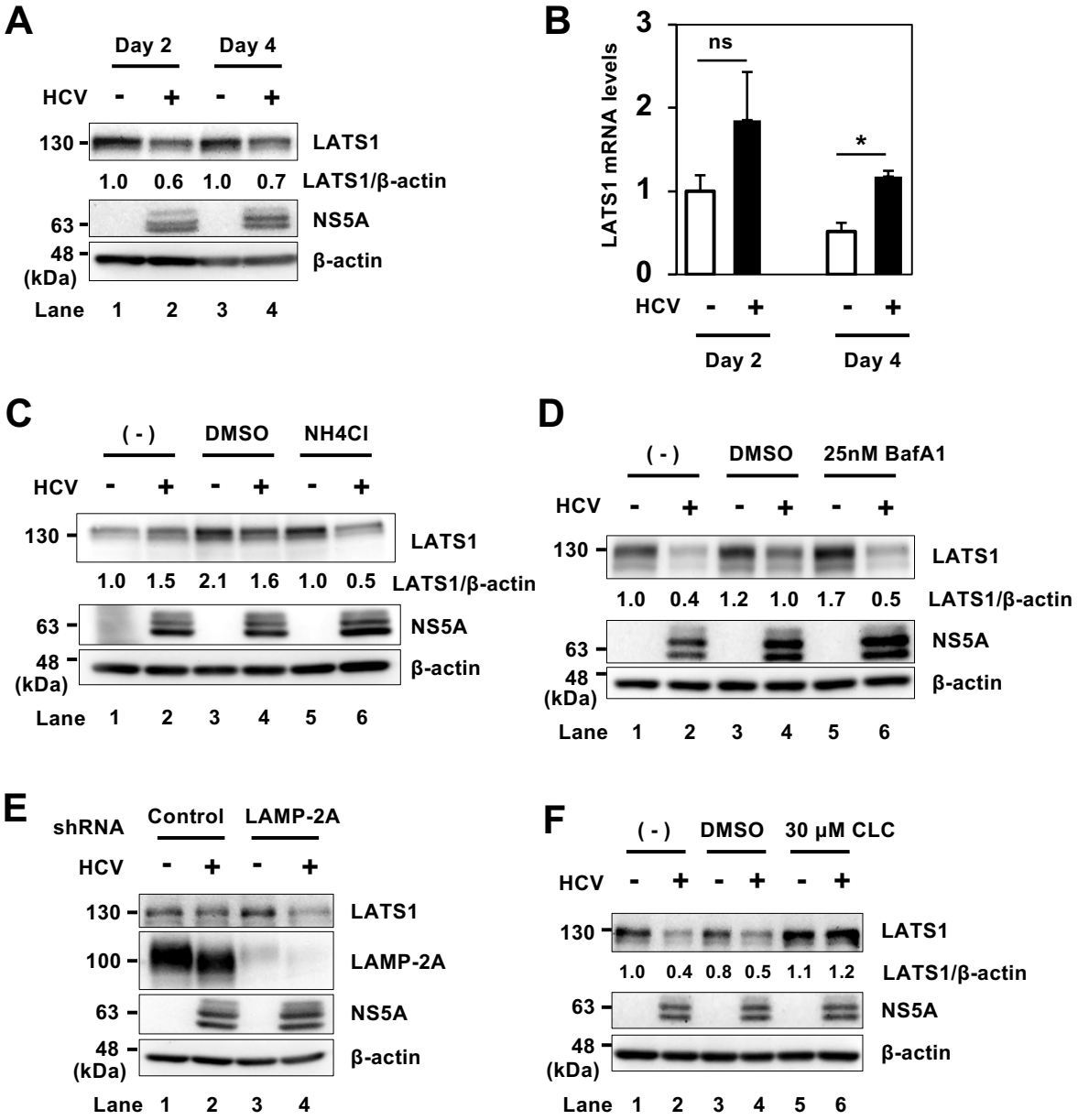

Fig. 1 Maria et al.

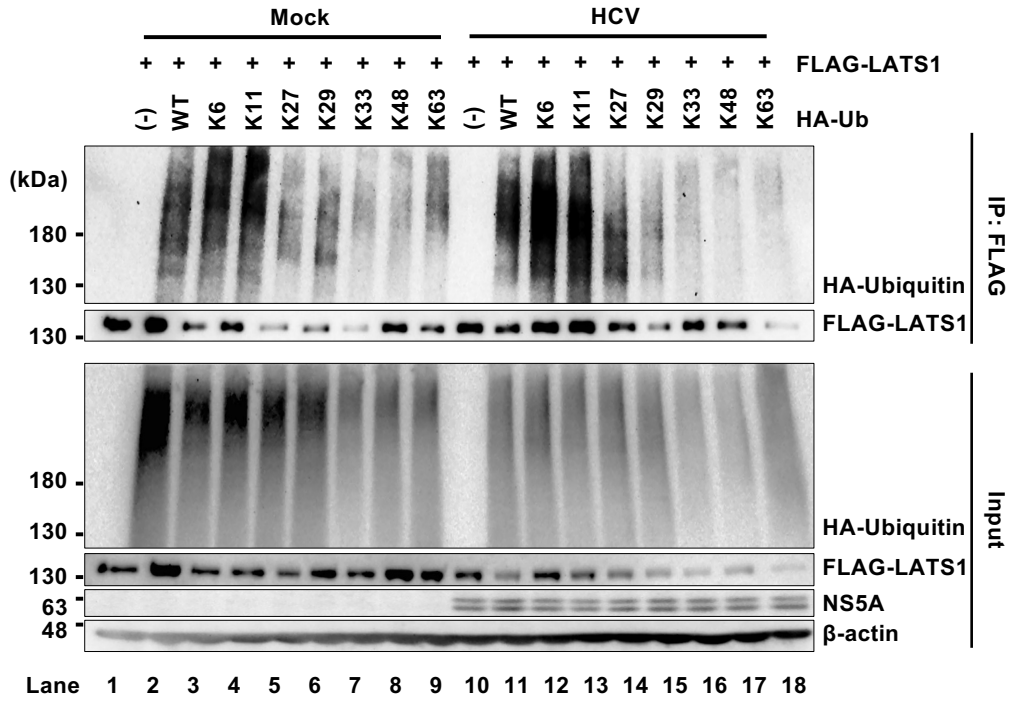

Fig. 2 Maria et al.

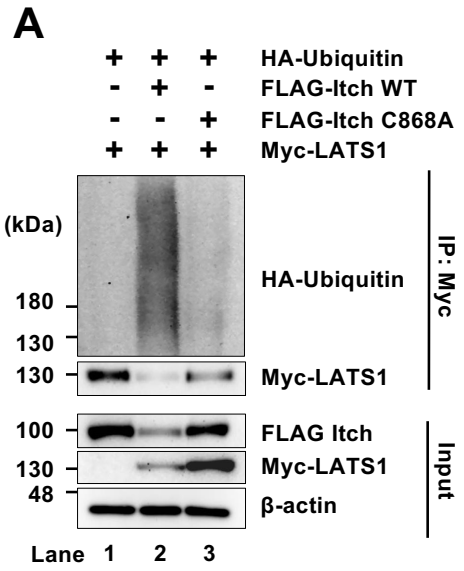

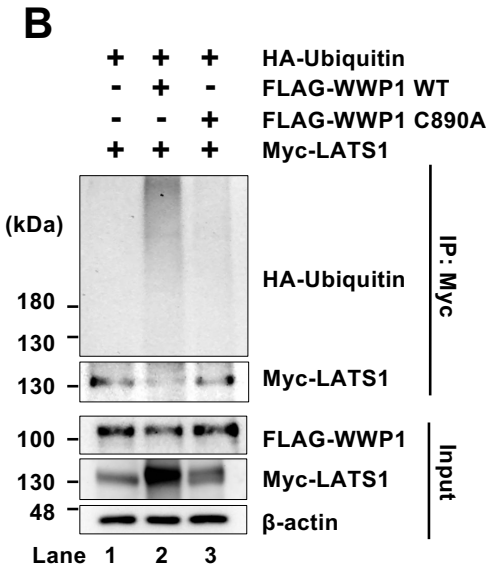

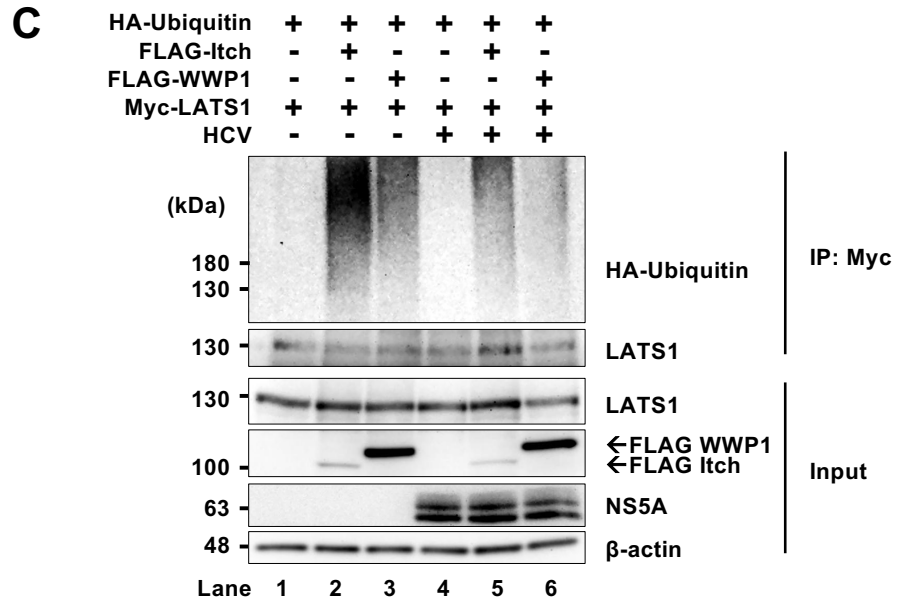

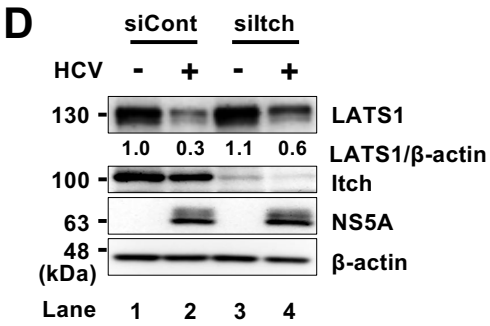

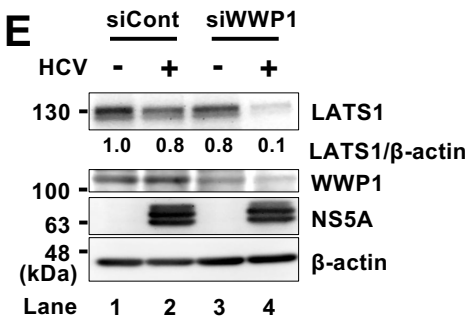

Fig. 3 Maria et al.

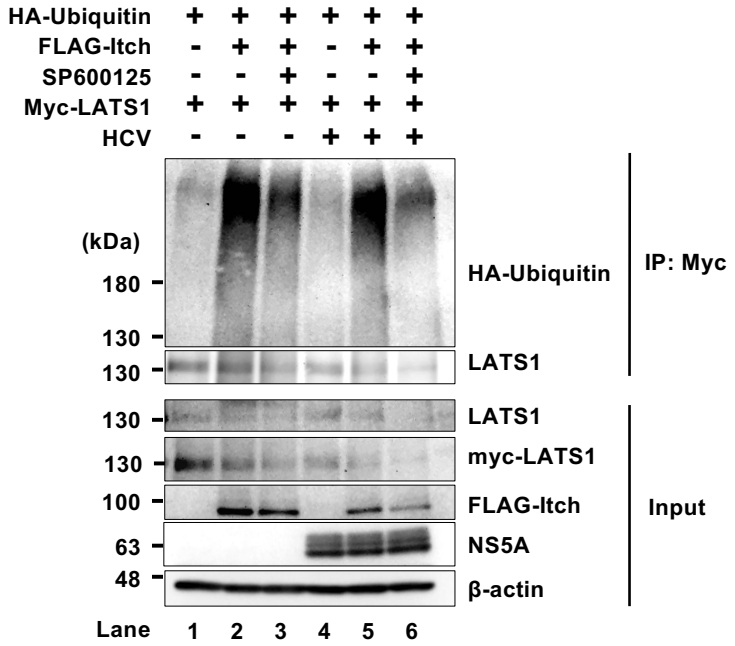

Fig. 4 Maria et al.

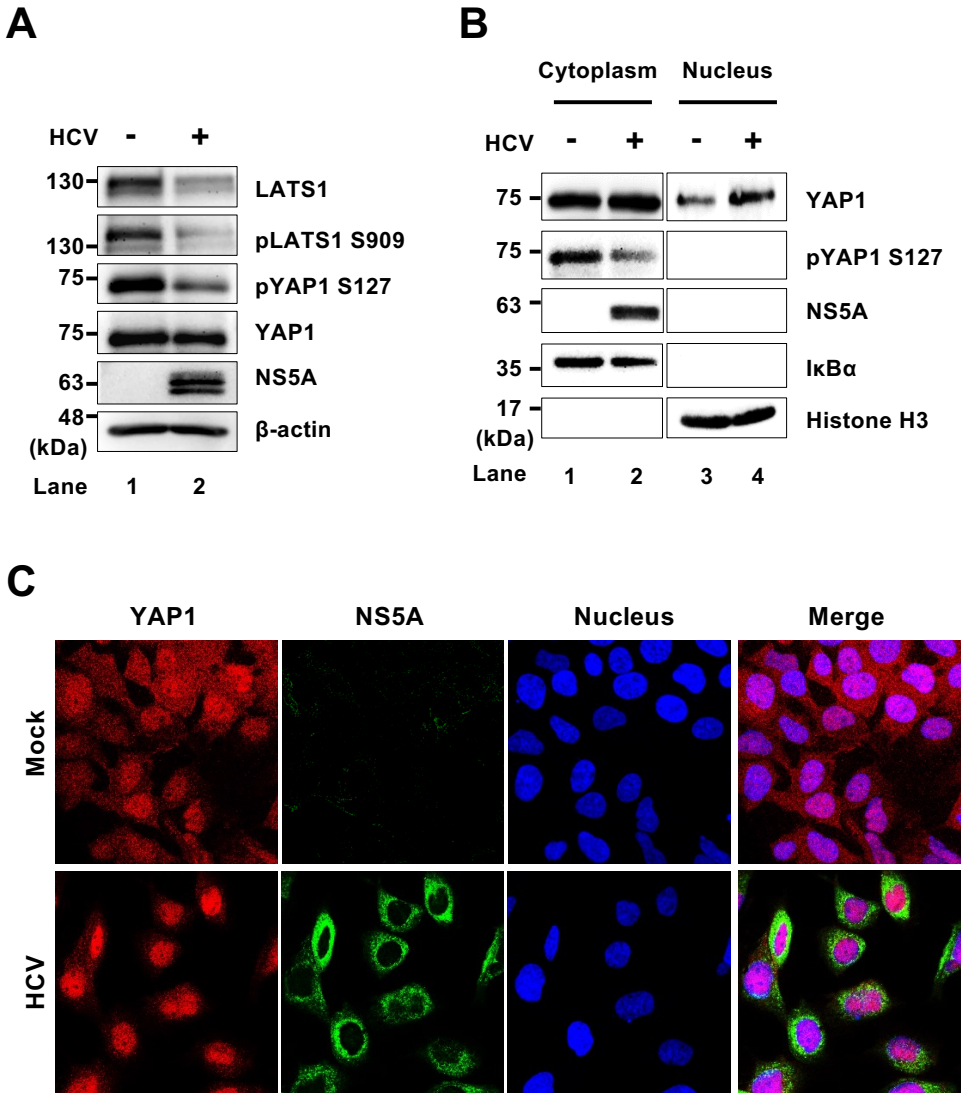

Fig. 5 Maria et al.

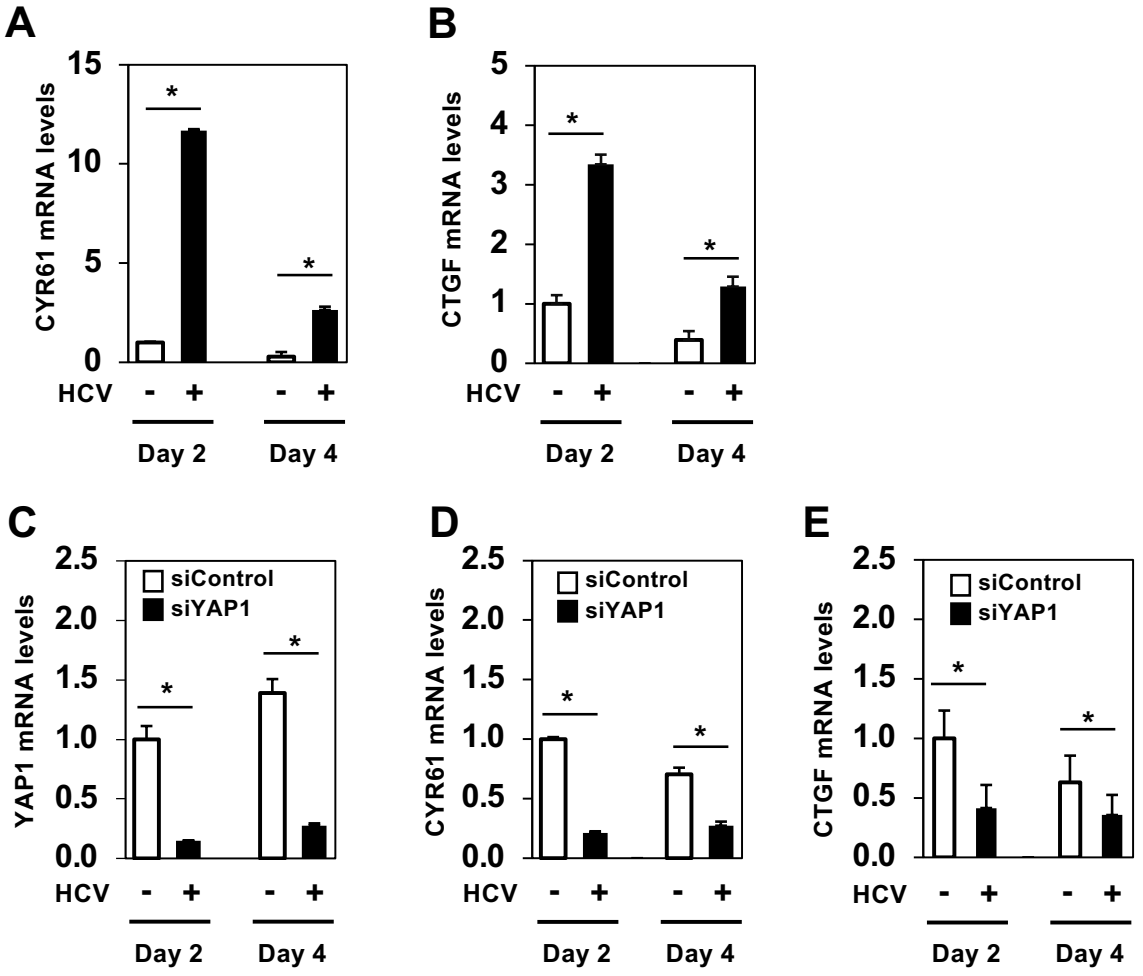

Fig. 6 Maria et al.

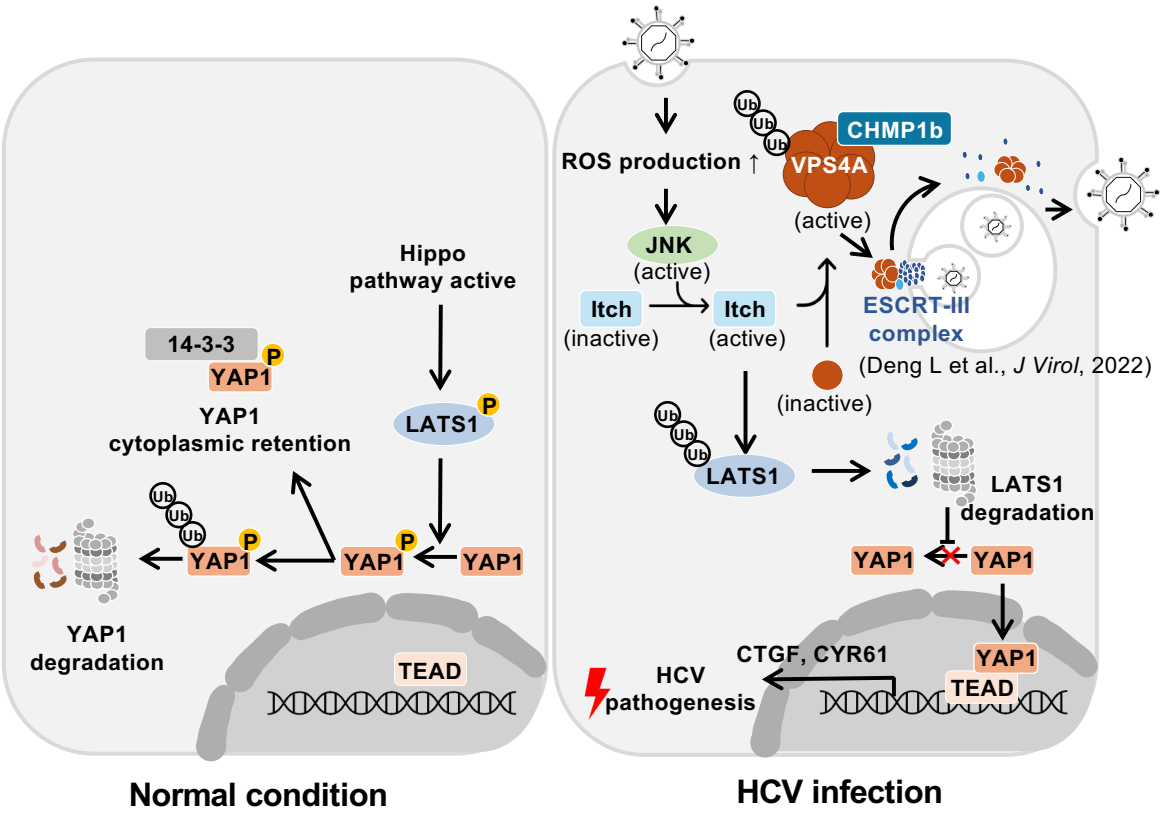

Fig. 7 Maria et al.